Cytocompatibility evaluation of gum Arabic-coated ultra-pure boron nitride nanotubes on human cells

The final version of this manuscript was published by Nanomedicine:

Cytocompatibility evaluation of gum Arabic-coated ultra-pure boron nitride nanotubes on human cells

Gianni Ciofani, Serena Del Turco, Antonella Rocca, Giuseppe de Vito, Valentina Cappello, Maho Yamaguchi, Xia Li, Barbara Mazzolai, Giuseppina Basta, Mauro Gemmi, Vincenzo Piazza, Dmitri Golberg, and Virgilio Mattoli

Nanomedicine 2014 9:6, 773-788

Cytocompatibility evaluation of gum Arabic coated ultra-pure boron nitride nanotubes on human cells

Gianni Ciofani[1*], Serena Del Turco[2], Antonella Rocca[1,3], Giuseppe de Vito[4,5], Valentina Cappello[4], Maho Yamaguchi[6], Xia Li[6], Barbara Mazzolai[1], Giuseppina Basta[2], Mauro Gemmi[4], Vincenzo Piazza[4], Dmitri Golberg[6], Virgilio Mattoli[1]

1 Istituto Italiano di Tecnologia, Center for Micro-BioRobotics @SSSA, Viale Rinaldo Piaggio 34, 56025 Pontedera (Pisa), Italy

2 CNR, Institute of Clinical Physiology, Via Moruzzi 1, 56124 Pisa, Italy

3 Scuola Superiore Sant'Anna, The BioRobotics Institute, Viale Rinaldo Piaggio 34, 56025 Pontedera (Pisa), Italy

4 Istituto Italiano di Tecnologia, Center for Nanotechnology Innovation @NEST, Piazza San Silvestro 12, 56127 Pisa, Italy

5 Scuola Normale Superiore, NEST, Piazza San Silvestro 12, 56127 Pisa, Italy

6 National Institute for Materials Science (NIMS), International Center for Materials Nanoarchitectonics (MANA), Namiki 1-1, 305-0044 Tsukuba (Ibaraki), Japan

*Corresponding Author

Gianni Ciofani, Ph.D.

Istituto Italiano di Tecnologia

Center for Micro-BioRobotics @SSSA

Viale Rinaldo Piaggio 34, 56025 Pontedera (Pisa), Italy

Tel. +39050883019

Lab. +39050883027

Fax +39050883497

EMail gianni.ciofani@iit.it

Abstract

Aims. Boron nitride nanotubes (BNNTs) are tubular nanoparticles with a structure analogue to that of carbon nanotubes, but with B and N atoms that completely replace the C atoms. Many favorable results indicate BNNTs as safe nanomaterials, however, important concerns have recently been raised about ultra-pure, long (~10 μm) BNNTs tested on several cell types. Materials & Methods. Here, we propose additional experiments with the same BNNTs, but made shorter (~1.5 μm) with a homogenization/sonication treatment that allows for their dispersion in gum Arabic aqueous solutions. Obtained BNNTs are tested on human endothelial and neuron-like cells with several independent biocompatibility assays. Moreover, for the first time, their strong sum-frequency generation signal is exploited to assess the cellular up-take. Results and Conclusions. Our data demonstrate no toxic effects up to concentrations of 20 μg/ml, once more confirming biosafety of BNNTs, and again highlighting that nanoparticle aspect ratio plays a key role in the biocompatibility evaluation.

Keywords

Boron nitride nanotubes; gum Arabic; SH-SY5Y; HUVECs; biocompatibility.

1. Introduction

Boron nitride nanotubes (BNNTs) gained huge interest in the latest decades because of their peculiar chemical and physical properties [1]. Applications in nanotechnology are nowadays well established, and in biomedicine they have been recently considered for a wide variety of potential applications, that range form drug delivery systems [2] to intracellular nanotransducers [3].

However, in order to actually exploit innovative nanoparticles in biomedicine, their biocompatibility has to be mandatory assessed, in particular in the case of inorganic nanoparticles. As we have recently reviewed [4], in the past years we assisted to increasing studies about interactions between BNNTs and living matter. Most important researches have highlighted no adverse effects following BNNT administration to several cell lines, including human embryonic kidney cells HEK 293 and Chinese hamster ovary cells CHO [2], human osteoblasts and mouse macrophages [5], human neuroblastoma cells SH-SY5Y [6], mouse myoblasts C2C12 [7], and neuronal-like PC12 cells [3]. Moreover, good results in terms of *in vivo* toxicological investigation [8-9] have been recently pointed out.

Despite these positive results, a comprehensive study by Horvàth and collaborators pointed out a relevant toxicity of BNNTs, tested on several cell lines, including lung epithelium cells, mouse macrophage cells, mouse embryonic fibroblasts, and human embryonic kidney cells. The main difference between the BNNTs investigated in this research and those one that resulted safe and biocompatible is represented by the length of the nanotubes themselves and, therefore, by their aspect ratio: in particular, the BNNTs tested in the study of Horvàth *et al.* are much longer (length $\geq$ 10 μm) than those previously tested, with a huge aspect ratio, and this is, in our opinion, the main reason of poor biocompatibility, as already reported for other kinds of nanomaterials [10].

In order to test this hypothesis, here we propose a set of biocompatibility tests of the same BNNTs used in the work of Horvàth *et al.*, but made shorter thanks to a dedicated procedure. Obtained BNNT dispersions have been thereafter tested on two human cell models: neuroblastoma SH-SY5Y cells, and human umbilical vein endothelial cells (HUVECs).

Results are encouraging and demonstrated a good response of both kind of cells towards ultra-pure, shortened (about 1.5 μm) BNNTs: the latter strongly interact with the cells and are eventually internalized, without affecting cell metabolism, proliferation and function up to concentrations of 20 μg/ml, that represent a satisfactory value for many biomedical applications [11].

2. Materials and methods

2.1 Boron nitride nanotubes dispersion preparation and characterization

High-purity multi-walled BNNTs were synthesized by a carbon-free chemical vapor deposition technique, by using boron and metal oxides as reactants at about 1500 °C [12]. Previous characterizations highlighted almost perfect crystalline structures [13], lengths up to 10 μm, and external diameters in the range of 10-80 nm [14]. The product purity at the end of the synthesis procedure resulted extremely high (> 90 wt%).

Gum Arabic (Sigma) was used for the dispersion and stabilization of BNNTs [15]. Dispersions were prepared with phosphate buffered solution (PBS). Briefly, BNNTs (1 mg) were mixed with 1 ml of a 0.1% gum Arabic solution in a polystyrene tube, thus obtaining a 1:1 (w/w) BNNT/gum Arabic ratio. In order to obtain an efficient disentanglement of the BNNT bundles, the mixture was homogenized for 15 min at 30000 rpm with a homogenizer (T10 basic, UltraTurrax). The samples were thus sonicated for 24 h (by a Bransonic

sonicator 2510) using an output power of 20 W for all the experiments, in order both to improve the BNNT dispersion, and to significantly shorten the nanotube length.

The obtained BNNT dispersions in gum Arabic solutions were characterized by scanning electron microscopy through a Dual-Beam system (FEI Helios 600), by dropping a small quantity of diluted dispersion on a silicon wafer, gold-sputtered before observation. Analysis of BNNT length after the dispersion procedure was performed with ImageJ software (http://rsb.info.nih.gov/ij/) on acquired SEM images (at least 200 nanotubes were considered for statistical analysis purpose).

2.2 Cell cultures

Human neuroblastoma SH-SY5Y cells (ATCC CRL-2266) were cultured in Dulbecco's modified Eagle's medium (DMEM) and Ham's F12 (1:1) with 10% fetal bovine serum, 100 IU/ml penicillin, 100 μg/ml streptomycin, and 2 mM L-glutamine. Cells were maintained at 37°C in a saturated humidity atmosphere containing 95% air / 5% CO_2.

Differentiation of SH-SY5Y cells was induced incubating cells (10,000 /cm^2) with a low-serum medium (DMEM with 1% fetal bovine serum, 100 IU/ml penicillin, 100 μg/ml streptomycin, and 2 mM L-glutamine) supplemented with 10 μM of all-trans retinoic acid.

Primary human umbilical vein endothelial cells (HUVECs) were isolated by type 2 collagenase digestion as already described [16], and used within third passage. They were treated in conformance with the principles outlined in the Declaration of Helsinki, obtained from discarded umbilical veins, and treated anonymously, so with no necessity of the ethical approval from the University Board. Cells were cultured in flasks coated with 0.5% gelatin in medium 199 containing 100 IU/ml penicillin, 100 μg/ml streptomycin, 2 mM L-

glutamine, 20 ng/ml endothelial cell growth factors (ECGF), and 10% fetal bovine serum (FBS).

All cell culture reagents were purchased from BioWhittaker (Cambrex).

2.3 Viability testing

BNNT cytocompatibility on SH-SY5Y cells was evaluated through the WST-1 assay (2-(4-iodophenyl)-3-(4-nitophenyl)-5-(2,4-disulfophenyl)-2H-tetrazoilium monosodium salt, provided in a pre-mix electro-coupling solution, BioVision). Cells were seeded in 96-well plates (2,000 cells *per* well) and incubated with increasing concentrations of BNNTs (0, 10, 20, 50 and 100 μg/ml). After 24, 48, and 72 h of incubation cultures were treated with 100 μl of growth medium added with 10 μl of the pre-mix solution for further 2 h and, finally, absorbance was read at 450 nm with a microplate reader (Victor3, Perkin Elmer).

Viability on SH-SY5Y cells was further qualitatively investigated at 72 h with the Live/Dead® viability/cytotoxicity Kit (Molecular Probes). The kit contains calcein AM (4 mM in anhydrous DMSO) and ethidium homodimer-1 (EthD-1, 2 mM in DMSO/H_2O 1:4 (v/v)), and allows for the discrimination between live cells (stained in green by calcein) and dead cells (stained in red by EthD-1). Cultures were rinsed with PBS, treated for 10 min at 37°C with 2 μM calcein AM and 4 μM EthD-1 in PBS, and finally observed with an inverted fluorescence microscope (TE2000U, Nikon) equipped with a cooled CCD camera (DS-5MC USB2, Nikon) and with NIS Elements imaging software.

Amido Black assay was performed on HUVEC monolayer cultured for 24, 48, and 72 h with BNNT-doped medium (in the range 0-100 μg/ml). At the end-point, cells were fixed with 4% of paraformaldehyde and then incubated with Amido Black dye (Sigma) for 15 min.

After several washing steps, the dye was extracted with NaOH 50 mM, and the absorbance read at 620 nm with the microplate reader.

Intracellular reactive oxygen species (ROS) generation was measured with the fluorescent dye 6-carboxy-2′,7′-dichlorodihydrofluorescein diacetate bis(acetoxymethyl)-ester (C-DCF-DA; Molecular Probes). C-DCFH-DA rapidly penetrates cell membrane and becomes deacetylated by endogenous esterases to form the non-fluorescent 2',7'-dichlorfluorescein (DCFH). DCFH is thereafter converted to green fluorescent dichlorofluorescein (DCF) compound by the action of cellular oxidants. Briefly, HUVEC monolayers were incubated with BNNTs for 24 and 48 h, then washed with phenol red-free Hanks'-buffered saline and incubated with C-DCF-DA (25 μM) for 30 min at 37°C, in Hank's buffer. After this step, cells were washed and scraped off into 1 ml of distilled water, sonicated and centrifuged. The fluorescence of supernatants was measured with a spectrofluorometer at 485 nm excitation and 525 nm emission, and data of three independent experiments were expressed in fluorescence arbitrary units. Positive control experiments were performed with an incubation of 30 min with H_2O_2 50 μM.

Quantification of apoptosis following BNNT incubation was investigated on HUVECs by using an annexin V-FITC/propidium iodide (PI) apoptosis detection kit (Sigma) according to the manufacturer's instructions. Briefly, after BNNT treatment (0 and 20 μg/ml for 24, 48 and 72 h), HUVECs were collected, washed with PBS twice, resuspended in 1× binding buffer and subjected to FITC-conjugated annexin V and propidium iodide (PI) staining for 10 min at room temperature in the dark. After staining, samples were assayed by flow cytometry (BD Accuri™ C6) for the quantification of apoptotic cells. For each sample, 15000 total events were analyzed. The assay allowed viable (negative for both annexin-V FITC and PI staining), necrotic (negative for annexin-V FITC and positive for PI), early

apoptotic (positive for annexin-V FITC and negative for PI), and late apoptotic cells (positive for both annexin-V FITC and PI) to be quantified.

2.4 Cell/BNNT interaction investigation

Study of cytoskeleton configuration following BNNT treatment was performed through f-actin staining with TRITC-phalloidin, according to the following procedure. After incubation with 20 μg/ml of BNNTs, cells (5000 /cm^2) were fixed with a 4% paraformaldehyde solution in PBS for 20 min at 4°C. Thereafter, they were rinsed with PBS and treated with a 0.1% Triton X-100 (Sigma) solution in PBS for 15 min to permeabilize cell membrane. Saturation was allowed for 30 min, using 0.1% goat serum in PBS, then incubation with a 100 μM solution of TRITC-phalloidin (Sigma) and 1 μM DAPI for nuclei blue counterstaining was performed for 45 min. Samples were finally rinsed with PBS and thus observed with a confocal laser scanning microscope (C2s, Nikon).

The interaction between BNNTs and SH-SY5Y cells was further investigated through SEM imaging. Cell cultures treated as previously described were fixed with two sequential incubations with a 4% paraformaldehyde solution (at 4°C for 30 min) and with a 2.5% glutaraldehyde solution (at 4°C for 2 h). Samples were then dehydrated through an ethanol gradient (0, 25, 50, 75 and 100%), overnight dried, and gold-sputtered before SEM observation through a Dual-Beam system (FEI Helios 600).

Nanoparticle internalization has been investigated in cells treated for 24 h with 20 μg/ml of BNNTs by a multimodal microscope with an in-plane resolution of approximately 300 nm and a resolution of 1 μm along the optical axis. Coherent Anti-Stokes Raman Scattering (CARS) has been exploited to obtain images of cells, based on a degenerate pump-and-probe beam (PaPB), created by a Ti-Sa pulsed laser (Coherent Chameleon Vision II) and a

supercontinuum generator (SCG, photonic-crystal fiber SCG-800 Newport) that generates a broadband Stokes beam. To maximize the spectral resolution, the beams were optimally chirped [17] by propagating them through two SF6-glass blocks, a 10 cm long one for the PaPB and a 15 cm long one for the Stokes radiation. The delay between the PaPB and the Stokes beam was adjusted in order to excite CH_2 bonds at a Raman shift of 2850 cm^{-1} and to permit imaging of the cells. Sum-Frequency Generation (SFG) signal originating from the BNNTs at approximately 450 nm by the combination of 800 nm PaPB with Stokes photons allowed the localization of BNNTs inside the cells.

BNNT internalization by HUVECs was instead investigated through transmission electron microscopy (TEM). Control and treated (20 μg/ml of BNNTs for 24 h) HUVEC cultures were fixed as monolayer with a solution of 2% glutaraldehyde in cacodylate buffer. Thereafter, cells were scraped, centrifuged and treated as pellet with a standard embedding protocol. Briefly, samples were post-fixed in 2% osmium tetroxide in cacodylate buffer, rinsed, and stained *en bloc* with uranyl acetate statured solution in ethanol 20%. Finally, samples were dehydrated and embedded in epoxy resin (Epon 812, Electron Microscopy Science), that was baked for 48 h at 60°C. Thin sections of 90 nm thickness were cut with a UC7 Leica ultramicrotome and collected on copper grids 300 meshes. TEM analyses were performed with a Zeiss Libra 120 plus electron microscope.

2.5 SH-SY5Y differentiation: immunofluorescence and qRT-PCR

Differentiation of SH-SY5Y cells in the presence of BNNTs was evaluated performing cultures in differentiation medium, supplemented with 0, 20 and 50 μg/ml of BNNTs. After five days, differentiation was assessed through immunofluorescence analysis of β3-tubulin, a specific neuronal differentiation marker, and f-actin.

Cells were rinsed with PBS and fixed in paraformaldehyde (4% in PBS) for 20 min. After rinsing with PBS, they were incubated with sodium borohydryde (1 mg/ml in PBS) for 10 min to reduce autofluorescence. Cellular membranes were then permeabilized with 0.1% Triton X-100 in PBS for 15 min. Antibody aspecific binding sites were saturated with 10% goat serum in PBS for 1 h, and, subsequently, a primary antibody (rabbit polyclonal IgG anti-tubulin, Sigma, diluted 1:75 in 10% goat serum) was added. After 30 min of incubation at 37°C, samples were rinsed with 10% goat serum; then, a staining solution was added, composed of a secondary antibody (fluorescent goat anti-rabbit IgG, Invitrogen) diluted 1:250 in 10% goat serum, of 100 μM of TRITC-phalloidin (Sigma) for f-actin staining, and of 1 μM DAPI for nucleus counterstaining. After 30 min of incubation at room temperature, samples were rinsed with 0.45 M NaCl in PBS for 1 min to remove weakly bound antibodies and, after rinsing in PBS, observed with the inverted fluorescence microscope.

The gene transcription levels of specific markers of neuronal cell maturation (laminin, *Lam*; microtubule-associated protein 2, *Map2*; neurogenic differentiation factor 1, *NeuroD1*; β3-tubulin, *TubB3*) were moreover evaluated with quantitative real-time RT-PCR (qRT-PCR). Total RNA was isolated from cell cultures using High Pure RNA Isolation kit (Roche) according to the manufacturer's protocol. Retro-transcription into cDNA was performed with 400 ng of RNA in a total volume of 20 μl, including 4 μl of iScriptTM Reverse Transcription Supermix (5X, Bio-Rad). The synthesis program included an initial incubation at 25°C for 5 min, followed by incubation at 42°C for 45 min and at 48°C for 15 min. After inactivation of the reaction by heating at 85°C for 5 min, the samples were increased up to 200 μl with pure distilled water (MilliQ, Millipore).

Quantitative RT-PCR was performed with a CFX Connect™ Real-Time PCR Detection System (Bio-Rad). Results were normalized to the transcription levels of a selected

housekeeping gene, glyceraldehyde 3-phosphate dehydrogenase (*Gapdh*). The obtained cDNA (5 µl) was mixed with 1 µl of specific forward and reverse primers (8 µM), 4 µl of MilliQ, and 10 µl of SsoAdvancedTM SYBR®Green Supermix (Bio-Rad). The thermal protocol was applied with one cycle of 30 s at 98°C and 40 cycles at 98°C for 3 s and 60°C for 7 s. At the end of amplification, a temperature ramp from 65°C to 95°C, with 0.5°C/s increments was performed, to exclude unspecific products through melting curve results analysis. Each assay included "no template" sample and all tests were carried out in triplicate. The cycle threshold (Ct) value relative of control sample was adopted as reference for the calculation of ΔΔCt (difference between ΔCt values deriving from difference between Ct of target and housekeeping gene) for the subsequent samples. Primer sequences (forward and reverse) of the investigated genes are reported in Table 1.

2.6 Detection of endothelial adhesion molecule expression

Vascular cell adhesion molecule (VCAM)-1 and intercellular adhesion molecule (ICAM)-1 expression in HUVECs was assessed on cell monolayers incubated with increasing concentrations of BNNTs (0-100 µg/ml) for 18 h in 96-well microplates. Assessment of cell surface VCAM-1 and ICAM-1 was performed as described elsewhere [18] through cell surface enzyme immunoassay. Mouse anti-human monoclonal antibodies were used, namely anti–VCAM-1 IgG (Ab E1/6), and anti–ICAM-1 IgG (Ab HU5/3). Enzyme immunoassays were carried out by incubating the endothelial cell monolayers with saturating concentrations of specific monoclonal antibodies against the target molecule, followed by biotinylated goat anti-mouse IgG, and streptavidin-alkaline phosphatase (Amersham Life Sciences). The surface expression of each adhesion molecule was quantified reading absorbance at 405 nm with the microplate reader.

2.7 Statistical analysis

Data were analyzed using analysis of variance (ANOVA) followed by Bonferronis's *post-hoc* test to test for significance, that was set at $p < 0.05$, with the aid of KaleidaGraph (Sinergy Software); quantitative RT-PCR data were analyzed with the BioRad CFX Manager (BioRad); each experiment was performed in triplicate if not otherwise specified.

3. Results

3.1 BNNT characterization after gum Arabic dispersion

SEM investigation of BNNTs dispersed in gum Arabic denoted well dispersed nanostructures, as shown by low (Figure 1a) and high (Figure 1b) magnification images. Quantitative evaluation performed on single BNNTs (Figure 1c) revealed a monodisperse size, being 90% of BNNT length comprised between 1.2 and 2.2 μm, with a bell-shaped distribution and an average length of about 1.5 μm (Figure 1d).

Dispersions resulted stable for about one week since the preparation, when some precipitation could occur, easily avoided with a mild sonication for a few minutes.

3.2 Effects on SH-SY5Y cells

Proliferation of SH-SY5Y cells treated with BNNTs, evaluated in terms of metabolic activity by WST-1 assay, did not result statistically different from the control cultures at concentrations up to 20 μg/ml and after up to 72 h of incubation (Figure 2a). However, a significant decrement of cell proliferation was highlighted after 48 and 72 h of treatment for doses of 50 and 100 μg/ml ($p < 0.01$).

These results were confirmed by cell imaging with the Live/Dead® assay, that highlighted as cells failed to reach confluence, after 72 h of treatment, when incubated with 50 and 100 μg/ml (Figure 2b). No significant cell death (red cells) was highlighted for all the evaluated BNNT concentration, even if we cannot exclude detachment of dead cells at 50 and 100 μg/ml BNNT doses during the washing steps performed after the staining.

Qualitative examination of cytoskeletal f-actin was performed in order to verify any change in cytoskeleton organization and cellular shape after the BNNT treatment. As illustrated by confocal images reported in Figure 3a, no qualitative significant change in terms of cell morphology, cytoskeleton conformation, and nucleus shape and staining was noticed in SH-SY5Y cells treated with 20 μg/ml for 24 h with respect to the control. At high magnification, moreover, it has been possible to highlight internalization of BNNTs as reported in Figure 3b (BNNTs have been detected through light transmission channel and pseudo-colored in green after image-post processing).

Absence of any qualitative change in cell morphology was confirmed by SEM analysis carried out on control cultures (Figure 4a) and incubated for 24 h with 20 μg/ml of BNNTs (Figure 4b). Both images show polygonal cell bodies, well spread over the substrates and with several membrane protrusions (filopodia and lamellopodia) out of the cells. In samples treated with nanotubes, a strong association of the BNNTs with the cell membrane is evident, as shown in the inset of Figure 4b, where BNNTs appear interpenetrated with the membrane, suggesting a subsequent nanoparticle internalization (at least 50 cells *per* culture sample have been imaged, reported examples are representative of the considered experimental condition).

The latter has been in fact demonstrated thanks to the SFG signal by BNNTs. Figure 5a shows the emission spectrum from a bundle of nanotubes when illuminated with the pump-

and-probe and the Stokes beams, in the same conditions used for CARS imaging, except for the pump-and-probe beam being centered at 806 rather than 800 nm. Four distinct bands are discernible (from left to right in the Figure 5a) originating from: second-harmonic generation (SHG, labeled with *) from the 806-nm beam, SFG (labeled with #) from the combination of the 806 nm beam and the portion of the Stokes beam temporarily overlapping to it (*i.e.*, corresponding to approximately 1045 nm), broadband SHG (labeled with +) from the Stokes beam, and non-resonant CARS signal (labeled with §). SHG when the system was excited at 800 nm was generated outside our detection window. The inset shows a superposition of an image obtained with a transmitted-light microscope of a nanotube bundle and the detected SFG signal.

Figure 5b depicts instead results of internalization assessment: a *Z*-stack acquisition on a small area of a culture incubated for 24 h with 20 μg/ml of BNNTs is reported, where the green channel maps the intensity of the CARS signal, and the red channel indicates the intensity of the SFG signal. Dark spots are shadows of BNNTs below or above the imaging plane. Finally, in Figure 5c a single Z-slice, along a side projection, is provided, clearly showing BNNTs inside the cells.

Differentiation of SH-SY5Y in the presence of BNNTs was finally assessed. Figure 6a shows immunostaining of β3-tubulin (in green) and f-actin (in red) of cultures treated with 0, 10 and 20 μg/ml of BNNTs. Nanoparticles did not negatively affect the differentiation process at the tested concentrations: in all the cultures about 35% of the cells resulted positive for β3-tubulin staining and, therefore, exhibited neuronal-like phenotype.

The gene transcription levels of neuronal differentiation specific markers were finally evaluated with qRT-PCR, that highlighted as expression of *Lam*, *Map2*, and *TubB3* was not affected by the treatment with BNNTs. Instead, a significant up-regulation of *NeuroD1*

(about 2-fold, $p < 0.05$) was found in cultures differentiated in presence of 20 µg/ml of BNNTs.

3.3 Effects on HUVECs

Integrity of HUVEC monolayer was assessed in terms of total cellular protein content evaluation with the Amido Black assay, that revealed no negative effects up to 20 µg/ml of BNNTs and up to 72 h of treatment. Instead, concentrations of 50 and 100 µg/ml provided a significant ($p < 0.05$) decrement of protein content in the cell cultures, highlighting a possible damage of the cell monolayer (Figure 7a); however, observation under optical microscope at the end-point of incubation for all tested concentrations did not show any evident alteration of cell morphology and cell monolayer integrity compared to the controls.

Fluorescence detection of ROS in HUVECs treated with BNNTs demonstrated that nanotubes did not induce significant oxidative stress after up to 48 h of incubation, demonstrating .values comparable to those of the control cultures (Figure 7b, positive control with H_2O_2, not reported in the plot for better clarity, gave a value of 702 ± 47 AU).

Concerning quantification of apoptosis, we did not detect any significant increment of necrotic, early apoptotic, and late apoptotic cells after a treatment with 20 µg/ml of BNNTs and up to 72 h of incubation, thus further excluding detrimental effects of BNNTs at this concentration on endothelial cells. Detailed data of cytofluorimetric analysis are reported in Table 2.

Finally, in order to assess whether the incubation with BNNTs may foster HUVEC activation, surface expression of specific adhesion molecules was examined. As shown by graphs presented in Figure 8, BNNT treatment did not induce neither VCAM-1 (Figure 8a)

nor ICAM-1 (Figure 8b) expression at all the investigated concentrations, suggesting no alteration of endothelial physiology towards a pro-inflammatory state.

The ultrastructure of treated HUVECs was finally evaluated in comparison with untreated cells through TEM analysis. Concerning the presence of BNNTs in each cell, we could find from 2 to 5 aggregates *per* cell with an average number of 3 nanotubes *per* aggregate (Figure 9a and 9b), thus confirming that the internalization of BNNT is an efficient process. From a morphological point of view, not only the shape of the BNNTs observed inside the cells does not change compared to the BNNTs observed in suspension, but also their crystalline nature remains unaltered as confirmed by electron diffraction analysis (inset of Figure 9a). Nanotube diameter is the same (48 ± 12 nm inside the cells; 49 ± 10 nm outside the cells), but we observed that only BNNTs shorter than 1.5 μm could be efficiently internalized by the HUVECs.

Regarding intracellular localization, we observed that BNNTs never enter in the nuclear compartment; moreover, their cytoplasmatic distribution is random, without any preferential localization in cellular sub-compartments (Figure 9a). Cellular organelles are not affected by the administration of BNNTs, and their ultrastructure is perfectly comparable with what observed in control cells. In particular, we focused our attention on cytoskeleton structure in the close proximity of BNNTs, and none alteration was detected (Figure 9b). In a few cases we observed some lysosomes close to the BNNT aggregates, but without any appreciable sign of fagosomal pathway activation.

4. Discussion

Since a few years, our group pioneered biological investigations of BNNTs. Our findings, obtained with many different cell lines and, eventually, *in vivo*, pointed out a very good

response of biological systems towards BNNT administration. These results have been mainly achieved with relatively short BNNT (< 5 μm) obtained by using an annealing method from boron-containing precursors [19]. On the other hand, an important investigation carried out with BNNTs of about 10 μm, obtained by a carbon-free chemical vapor deposition technique, documented a rather strong toxicity of these nanomaterials [10].

Here, we have confirmed a hypothesis that the tube length plays a key role on BNNT toxicity, performing a cytocompatibility evaluation of the same BNNTs used by Horvàth and collaborators, but shortened through a dedicated procedure that involved their dispersion in gum Arabic, as already suggested by Gao *et al*. [15], that allowed well dispersed BNNTs, of length of about 1.5 μm, to be obtained. We carried out testing on SH-SY5Y and on HUVECs, that have already been positively tested with other types of BNNTs [6; 20].

SH-SY5Y is a human-derived cell line, that owns many features of catecholaminergic neurons, including expression of dopamine-β-hydroxylase, dopamine and acetylcholine receptor and transporters, and typical neuronal markers like neurofilament proteins [21]. SH-SY5Y well tolerated BNNT treatment up to 20 μg/ml, with no alteration of viability, proliferation, and differentiation capability with respect to the controls. BNNT internalization was confirmed by SEM, confocal, and multimodal imaging, combining CARS imaging and SFG, where CARS allowed imaging of the cell volume thanks to the abundance of CH_2 bonds, while SFG was exploited thanks to the strong non-linear properties of the BNNTs.

Gene analysis of specific neuronal maturation markers, moreover, revealed no alteration in transcription levels of genes coding for laminin, microtubule-associated protein 2, and βIII-tubulin. Laminin is one of the most important glycoprotein components of the basement membrane and it is involved in neuronal survival, differentiation, growth cone guidance, and

neurite growth [22]. Microtubule-associated protein 2 is instead involved in the stabilization of microtubules during neuronal development, and in the synthesis of other neuron-specific cytoskeletal element [23]. βIII-tubulin, finally, is a neuron-specific class of tubulin, and its expression in BNNT-treated differentiating SH-SY5Y was also confirmed by immunofluorescence [24]. Most interestingly, a significant up-regulation of gene coding for neurogenic differentiation factor 1 was highlighted by qRT-PCR in cells treated with 20 μg/ml. This is a helix-loop-helix transcription factor, involved in the growth and differentiation of neurons. It plays a key role in the neuronal development, both in the central [25-26] and in the peripheral nervous system [27-28]; moreover, it has been proven to be essential in the sustainment of neural precursor cells in adult neurogenesis [29-30]. We have already demonstrated as, in the presence of a mechanical stimulation, BNNTs are able to foster an improvement in PC12 cell differentiation [3]. Here, the up-regulation of *NeuroD1* was noticed just in the presence of BNNTs, without any kind of external stimulation: this result deserves future investigation, through a systematic study of the effects of BNNTs on neuronal cell development and differentiation, in order to assess any possible positive effects of these nanoparticles on neuronal cells, similarly to the case of carbon nanotubes [31-32].

Concerning testing on HUVECs, once again absence of negative effects have been demonstrated by analysis of the integrity of cell monolayer, by the absence of abnormal ROS production and apoptotic phenomena, and by the lack of increased expression of inflammatory markers like VCAM-1 and ICAM-1. Testing of nanomaterials on HUVECs is particular important: being vascular endothelium the first barrier that nanoparticles find after their intravenous injection [33], an evaluation of the interactions between endothelial cells and nanovectors can give important hints about their suitability in the clinical practice.

TEM analysis confirmed that BNNTs could be efficiently internalized by HUVECs, and that their internalization does not induce any morphological alteration in cell ultrastructure.

Collectively, all these results suggest that ultra-pure, gum Arabic-coated BNNTs are well tolerated by the tested human cells, and that the important cytotoxic effects highlighted by the previous study are very likely related to the BNNT length and to the huge aspect-ratio. This is in fact a key factor in nanoparticle toxicity, as already pointed out for other kind of nanoparticles. Concerning carbon nanotubes, for example, a direct correlation between nanotube length and asbestos-like pathogenic behavior was found [34], suggesting the phenomenon of "frustrated phagocytosis" as one of the possible mechanism of toxicity. More recently, a similar behavior has been highlighted with a completely different nano-system, namely nickel nanowires, that again showed a length-dependent pathogenicity in a mouse peritoneal model, where long nanofibers (> 20 μm) elicited strong inflammation that instead was not revealed in the case of treatment with < 5 μm nanowires [35].

Envisaging therapeutic applications, the possibility to further decrease the nanotube length down to sizes more amenable also for *in vivo* applications [36] will represent for sure a further step in order to achieve safe BNNT concentrations suitable for systemic administration.

5. Conclusion

Ultra-pure BNNTs have been dispersed in gum Arabic aqueous solutions, and made short (from ~10 μm to ~1.5 μm) thanks to a homogenization/sonication treatment. Obtained BNNT dispersions were well tolerated by both HUVECs and SH-SY5Y cells at concentrations up to 20 μg/ml, in terms of viability, proliferation, ROS production, lack of apoptosis, and other specific functionalities.

The selection of a suitable concentration range for nanoparticle safety assessment is not a trivial task [37-38]; however, these findings highlight that investigated BNNTs are suitable at reasonable high concentrations that could be useful for many bio-applications, as already proven in previous studies on other kinds of BNNTs [4] and on other nanoparticle systems [39-40]. Most importantly, we found the ultra-pure, short BNNTs are suitable for *in vitro* biomedical applications up to 20 μg/ml, on the contrary of their longer counterparts, that given detrimental effects already at a concentration of about 2 μg/ml [10]. Our results highlighted once more a positive interaction of BNNTs with living materials, and stress the importance of nanotube length and aspect ratio during biocompatibility evaluation.

Future perspective

Boron nitride nanotubes represent excellent candidates for bio-applications in the next future. In Authors' opinion, the assessment of their biosafety, of which the present study represents a fundamental step, will soon lead to impressive theranostic applications of these nanovectors [4].

Summary points

Preparation of short ultra-pure BNNTs

- Short BNNTs have been obtained through a homogenization-sonication approach, that allowed their stable dispersion in gum Arabic

Effects on SH-SY5Y cells

- Viability
  - Good cellular response up to 20 μg/ml

  - Unaltered (or even enhanced) cellular differentiation towards neurons, verified at both gene and protein level
- Cells/BNNTs interactions
  - Strong interaction with cellular membrane verified through SEM analysis
  - Internalization verified through confocal and multimodal (CARS and SHG) microscopy

Effects on HUVECs

- Viability
  - Good cellular response up to 20 μg/ml
  - No inflammatory or stress response at all tested concentrations
- Cells/BNNTs interactions
  - No alteration of cell ultrastructure
  - Internalization verified through TEM analysis

Figure and Table captions

Figure 1. SEM images at increasing magnifications (a-c) of BNNTs after treatment with gum Arabic; quantitative evaluation of BNNT length distribution (d).

Figure 2. WST-1 assay results of SH-SY5Y cells treated with 0-100 μg/ml of BNNTs for 24, 48 and 72 h (a); Live/Dead® staining performed after 72 h of treatment (b); * $p < 0.01$.

Figure 3. Confocal laser scanning microscopy images of f-actin and nucleus of cells treated for 24 h with 0 and 20 μg/ml of BNNTs (a); high magnification confocal images showing BNNT internalization (b).

Figure 4. SEM imaging of control cells (a) and of cells treated with 20 μg/ml of BNNTs for 24 h (b); the inset shows the strong association of BNNTs with the cell membrane.

Figure 5. Emission spectrum from a bundle of nanotubes when illuminated with the pump-and-probe and the Stokes beams (a): four distinct bands are discernible originating from: SHG (labeled with *) from the 806-nm beam, SFG (labeled with #) from the combination of the 806 nm beam and the portion of the Stokes beam temporarily overlapping to it (*i.e.*, corresponding to approximately 1045 nm), broadband SHG (labeled with +) from the Stokes beam, and non-resonant CARS signal (labeled with §). The inset shows a superposition of an image obtained with a transmitted-light microscope of a nanotube bundle and the detected SFG signal. Multimodal *Z*-stacking of SH-SY5Y cells treated for 24 h with 20 μg/ml of BNNTs: map of the intensity of the CARS signals from the CH_2 bonds in green, SFG from the nanotubes in red (b); single *Z*-slice, along a side projection, showing BNNTs inside the cells (single BNNT highlighted by a circle). Scale bar 10 μm.

Figure 6. Immunofluorescence analysis of SH-SY5Y cells differentiated for 5 days in the presence of increasing concentrations of BNNTs: β3-tubulin in green, f-actin in red (a); qRT-PCR evaluation of transcription of genes involved in SH-SY5Y differentiation following BNNT treatment (b); * $p < 0.05$.

Figure 7. Amido Black assay results of HUVECs treated with 0-100 μg/ml of BNNTs for 24, 48 and 72 h (a); ROS detection on HUVECs treated up to 48 h with the same BNNT concentrations (b). * $p < 0.05$.

Figure 8. Effects of a 18 h treatment of BNNTs (0-100 μg/ml) on endothelial VCAM-1 (a) and ICAM-1 (b) surface expression.

Figure 9. Low (a) and high (b) magnification TEM images of BNNTs internalized by HUVECs. Electron diffraction analysis of BNNTs showed in the inset of (a).

Table 1. Primer sequences for qRT-PCR analysis.

Table 2. Quantification of apoptosis in HUVECs exposed to 20 μg/ml of BNNTs for 24, 48, and 72h.

References

[1] Wang J, Lee CH, Yap YK. Recent advancements in boron nitride nanotubes. Nanoscale 2, 2028-2034 (2010).

[2] Chen X, Wu P, Rousseas M, *et al.* Boron nitride nanotubes are noncytotoxic and can be functionalized for interaction with proteins and cells. *J. Am. Chem. Soc.* 131: 890-891 (2009).

[3] Ciofani G, Danti S, D'Alessandro D, *et al.* Enhancement of neurite outgrowth in neuronal-like cells following boron nitride nanotube-mediated stimulation. *ACS Nano* 4, 6267–6277 (2010).

[4] Ciofani G, Danti S, Genchi GG, Mazzolai B, Mattoli V. Boron nitride nanotubes: biocompatibility and potential spill-over in nanomedicine. *Small* 9, 1672-1685 (2013).

[5] Lahiri D, Rouzaud F, Richard T, *et al.* Boron nitride nanotube reinforced polylactide-polycaprolactone copolymer composite: mechanical properties and cytocompatibility with osteoblasts and macrophages *in vitro*. *Acta Biomater.* 6, 3524-3533 (2010).

[6] Ciofani G, Danti S, D'Alessandro D, Moscato S, Menciassi A. Assessing cytotoxicity of boron nitride nanotubes: interference with the MTT assay. *Biochem. Bioph. Res. Co.* 394, 405-411 (2010).

[7] Ciofani G, Ricotti L, Danti S, *et al.* Investigation of interactions between poly-L-lysine coated boron nitride nanotubes and C2C12 cells: up-take, cytocompatibility and differentiation. *Int. J. Nanomed.* 5, 285-298 (2010).

[8] Soares DCF, Ferreira TH, Ferreira CDA, Cardoso VN, De Sousa EMB. Boron nitride nanotubes radiolabeled with ^{99m}Tc: Preparation, physicochemical characterization, biodistribution study, and scintigraphic imaging in Swiss mice. *Int. J. Pharmaceut.* 423, 489-495 (2012).

[9] Ciofani G, Danti S, Nitti S, Mazzolai B, Mattoli V, Giorgi M. Biocompatibility of boron nitride nanotubes: an up-date of *in vivo* toxicological investigation. *Int. J. Pharmaceut.* 444: 85-88 (2013).

[10] Horváth L, Magrez A, Golberg D, *et al. In vitro* investigation of the cellular toxicity of boron nitride nanotubes. *ACS Nano* 5, 3800-3810 (2011).

[11] Yildirimer L, Thanh NTK, Loizidou M, Seifalian AM. Toxicological considerations of clinically applicable nanoparticles. *Nano Today* 6, 585-607 (2011).

[12] Tang CC, Bando Y, Sato T, Kurashima K. A novel precursor for synthesis of pure boron nitride nanotubes. *Chem. Comm.* 12, 1290-1291 (2002).

[13] Zhi CY, Bando Y, Tang CC, Golberg D. Effective precursor for high yield synthesis of pure BN nanotubes. *Solid State Commun.* 135, 67-70 (2005).

[14] Zhi CY, Bando Y, Tang CC, Golberg D. Boron nitride nanotubes. *Mater. Sci. Eng. R* 70, 92-111 (2010).

[15] Gao Z, Zhi CY, Bando Y, Golberg D, Komiyama M, Serizawa T. Efficient disentanglement of boron nitride nanotubes using water-soluble polysaccharides for protein immobilization. *RSC Adv.* 2, 6200-6208 (2012).

[16] Ciofani G, Del Turco S, Genchi GG, D'Alessandro D, Basta G, Mattoli V. Transferrin-conjugated boron nitride nanotubes: Protein grafting, characterization, and interaction with human endothelial cells. *Int. J. Pharmaceut.* 436, 444-453 (2012).

[17] Pegoraro AF, Ridsdale A, Moffatt DJ, Jia Y, Pezacki JP, Stolow A. Optimally chirped multimodal CARS microscopy based on a single Ti:sapphire oscillator. *Opt. Expr.* 17, 2984-2996 (2009).

[18] Basta G, Lazzerini G, Massaro M, *et al.* Advanced glycation end products activate endothelium through signal-transduction receptor RAGE: a mechanism for amplification of inflammatory responses. Circulation 105, 816-822 (2002).

[19] Wang J, Gu Y, Zhang L, Zhao G, Zhang Z. Synthesis of boron nitride nanotubes by self-propagation high-temperature synthesis and annealing method. *J. Nanomater.* 540456 (2010).

[20] Del Turco S, Ciofani G, Cappello V, *et al.* Cytocompatibility evaluation of glycol-chitosan coated boron nitride nanotubes in human endothelial cells. *Colloid. Surface B* 111, 142–149 (2013).

[21] Constantinescu R, Constantinescu AT, Reichmann H, Janetzky B. Neuronal differentiation and long-term culture of the human neuroblastoma line SH-SY5Y. *J. Neural Transm.* 72, 17-28 (2007).

[22] Plantman S. Proregenerative properties of ECM molecules. *BioMed Research International* 981695 (2013).

[23] Korzhevskii DE, Karpenko MN, Kirik OV. Microtubule-associated proteins as indicators of differentiation and the functional state of nerve cells. *Neurosci. Behav. Physiol.* 42, 215-222 (2012).

[24] Cooke MJ, Zahir T, Phillips SR, *et al*. Neural differentiation regulated by biomimetic surfaces presenting motifs of extracellular matrix proteins. *J. Biomed. Mater. Res. A* 93, 824-832 (2010).

[25] Jahan I, Kersigo J, Pan N, Fritzsch B. Neurod1 regulates survival and formation of connections in mouse ear and brain. *Cell Tissue Res.* 341, 95-110 (2010).

[26] Mehmood R, Yasuhara N, Oe S, Nagai M, Yoneda Y. Synergistic nuclear import of NeuroD1 and its partner transcription factor, E47, *via* heterodimerization. *Exp. Cell Res.* 315, 1639-1652 (2009).

[27] Yang T, Kersigo J, Jahan I, Pan N, Fritzsch B. The molecular basis of making spiral ganglion neurons and connecting them to hair cells of the organ of Corti. *Hearing Res.* 278, 21-33 (2011).

[28] Jahan I, Pan N, Kersigo J, Fritzsch B. Beyond generalized hair cells: Molecular cues for hair cell types. *Hearing Res.* 297, 30-41 (2013).

[29] Kuwabara T, Hsieh J, Muotri A, *et al.* Wnt-mediated activation of NeuroD1 and retro-elements during adult neurogenesis. *Nat Neurosci.* 12, 1097-1105 (2009).

[30] Gao Z, Ure K, Ables JL, *et al.* Neurod1 is essential for the survival and maturation of adult-born neurons. *Nat Neurosci.* 12, 1090-1092 (2009).

[31] Fabbro A, Villari A, Laishram J, *et al.* Spinal cord explants use carbon nanotube interfaces to enhance neurite outgrowth and to fortify synaptic inputs. *ACS Nano* 6, 2041-2055 (2012).

[32] Fabbro A, Bosi S, Ballerini L, Prato M. Carbon nanotubes: Artificial nanomaterials to engineer single neurons and neuronal networks. *ACS Chem. Neurosci.* 3, 611-618 (2012).

[33] Farooq A, Whitehead D, Azzawi M. Attenuation of endothelial-dependent vasodilator responses, induced by dye-encapsulated silica nanoparticles, in aortic vessels. *Nanomedicine UK*. doi:10.2217/nnm.12.213 (2013)

[34] Poland CA, Duffin R, Kinloch I, *et al.* Carbon nanotubes introduced into the abdominal cavity of mice show asbestos-like pathogenicity in a pilot study. *Nat. Nanotech.* 3, 423-428 (2008).

[35] Poland CA, Byrne F, Cho WS, *et al.* Length-dependent pathogenic effects of nickel nanowires in the lungs and the peritoneal cavity. *Nanotoxicology* 6, 899-911 (2012).

[36] Moghimi SM, Hunter AC, Murrey JC. Long-circulating and target-specific nanoparticles: theory to practice. *Pharmacol. Rev*. 53, 283-318 (2001).

[37] Li X, Wang L, Fan Y, Feng Q, Cui FZ. Biocompatibility and toxicity of nanoparticles and nanotubes. *J. Nanomater.* 548389 (2012).

[38] Kong B, Seog JH, Graham LM, Lee SB. Experimental considerations on the cytotoxicity of nanoparticles. *Nanomedicine UK* 6, 929-941 (2011).

[39] Xiong HM. ZnO nanoparticles applied to bioimaging and drug delivery. *Adv. Mater.* 25, 5329-5335 (2013).

[40] Avti PK, Caparelli ED, Sitharaman B. Cytotoxicity, cytocompatibility, cell-labeling efficiency, and *in vitro* cellular magnetic resonance imaging of gadolinium-catalyzed single-walled carbon nanotubes. *J. Biomed. Mater. Res. A* 101, 3580-3591 (2013).

Reference annotations

[4]** Comprehensive review on biomedical applications of BNNTs.

[10]** Study pointing out adverse biological effects of BNNTs.

[14]** Comprehensive review on BNNT technology.

[2]* BNNTs as protein and gene carriers are proposed.

[3]* First study about BNNTs as biological nanotransducers.

[5]* First study about BNNT applications in tissue engineering.

[8]* First *in vivo* investigation of BNNTs.

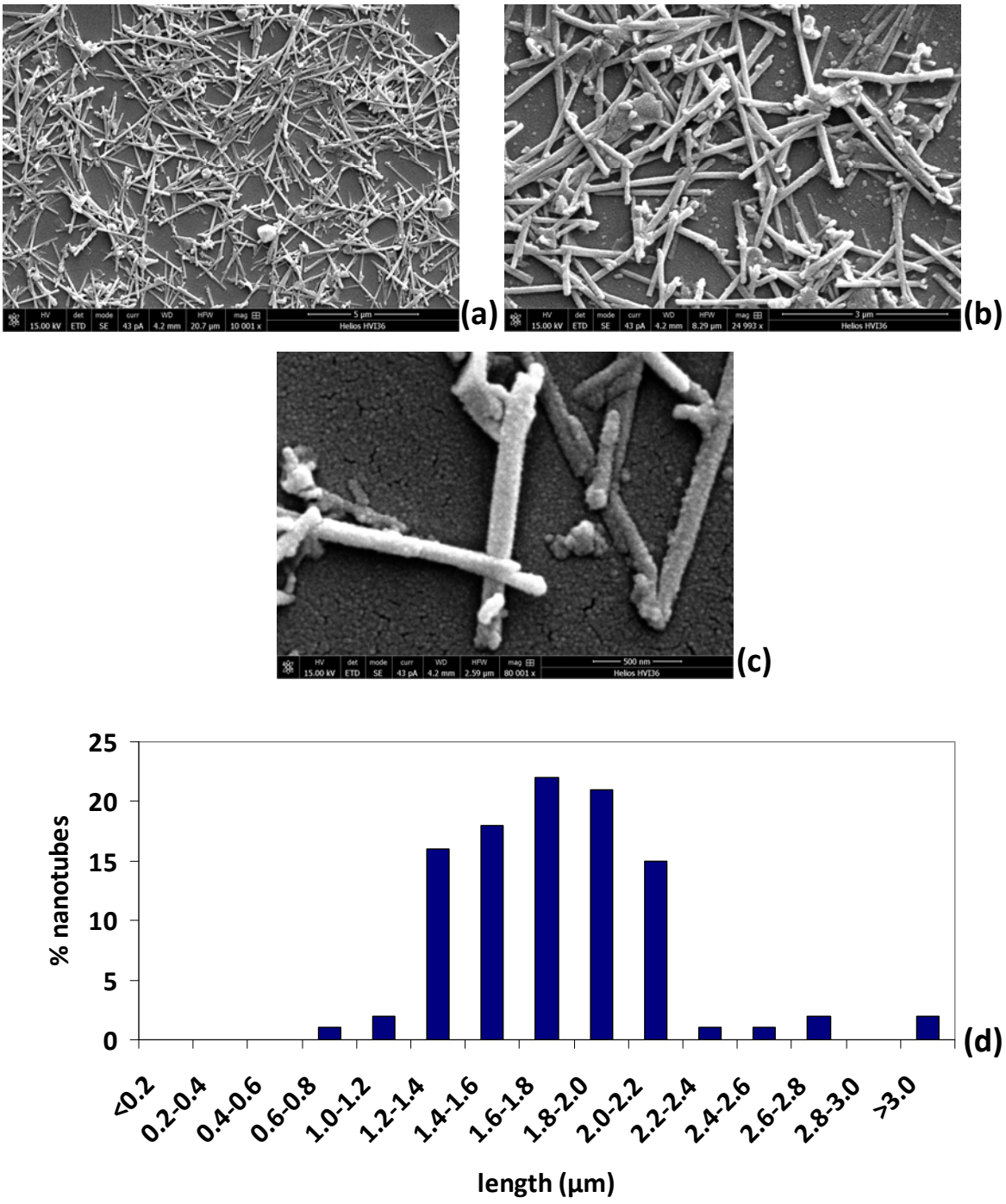

Figure 1. SEM images at increasing magnifications (a-c) of BNNTs after treatment with gum Arabic; quantitative evaluation of BNNT length distribution (d).

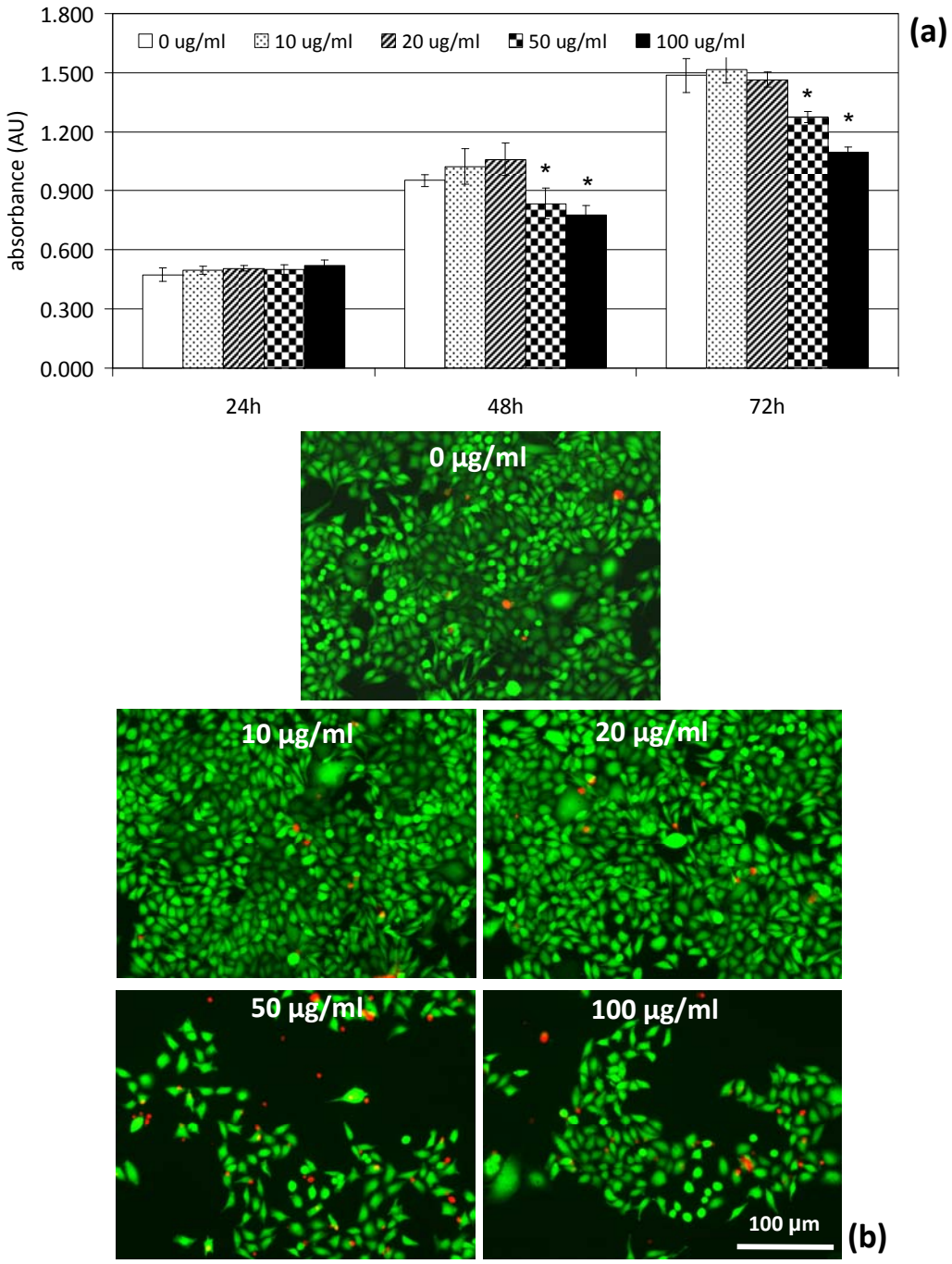

Figure 2. WST-1 assay results of SH-SY5Y cells treated with 0-100 µg/ml of BNNTs for 24, 48 and 72 h (a); Live/Dead® staining performed after 72 h of treatment (b).

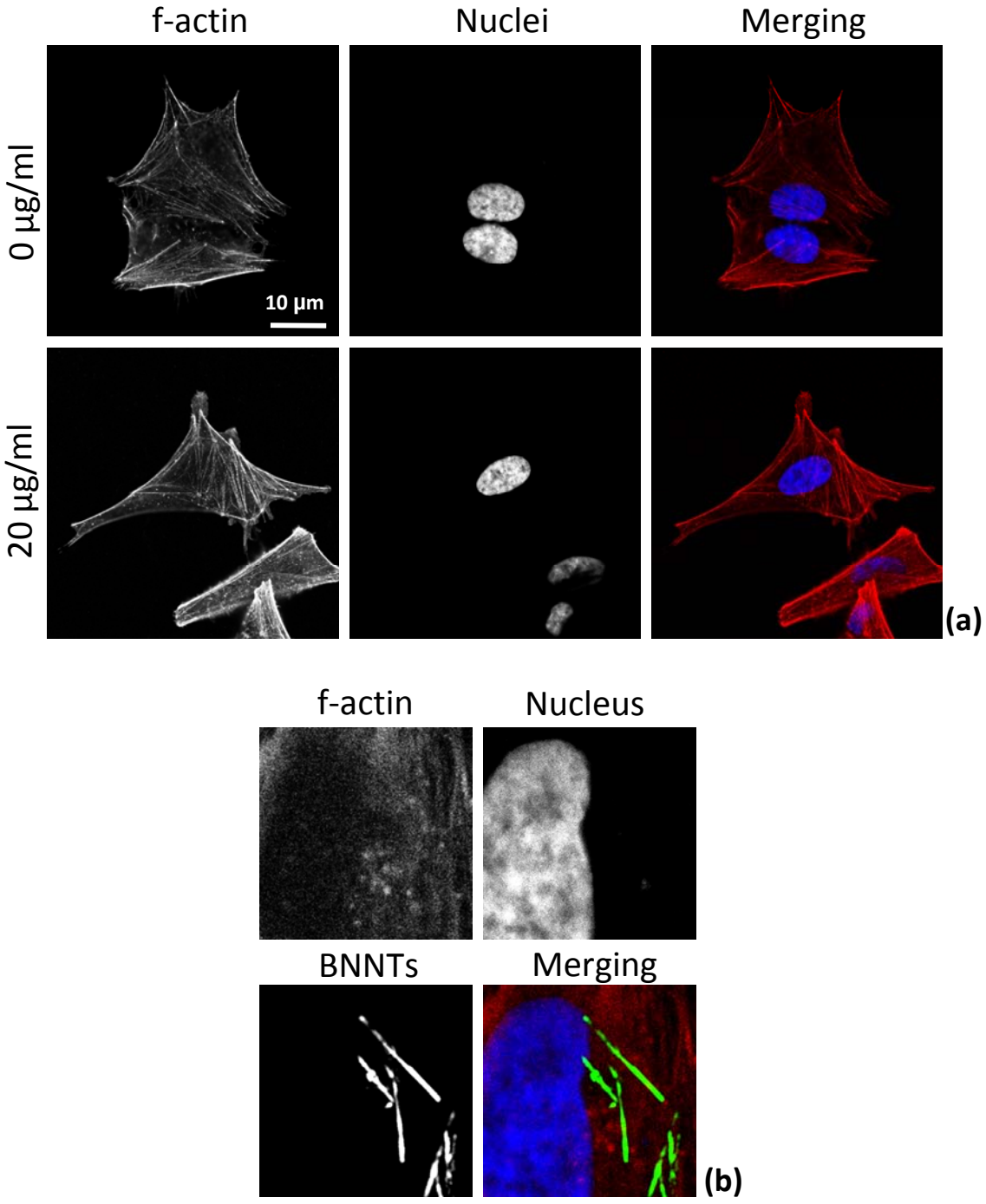

Figure 3. Confocal laser scanning microscopy images of f-actin and nucleus of cells treated for 24 h with 0 and 20 µg/ml of BNNTs (a); high magnification confocal images showing BNNT internalization (b).

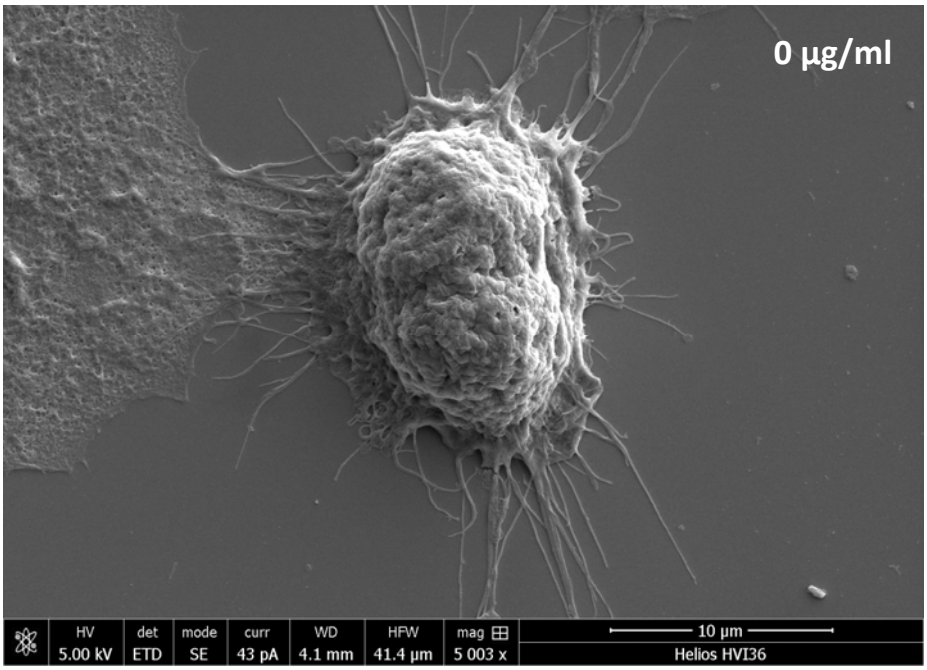

(a)

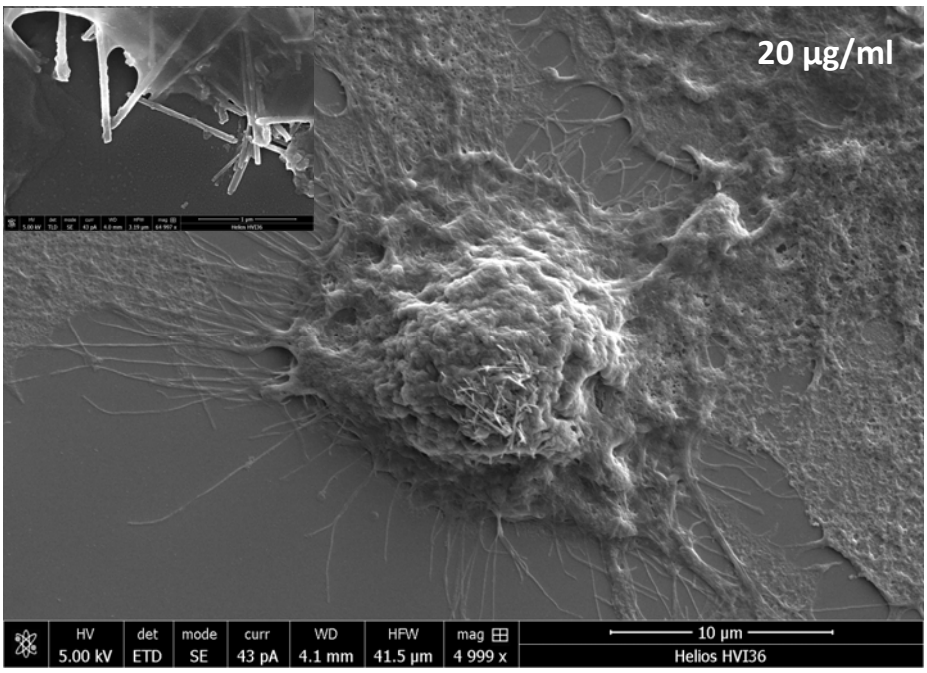

(b)

Figure 4. SEM imaging of control cells (a) and of cells treated with 20 µg/ml of BNNTs for 24 h (b); the inset shows the strong association of BNNTs with the cell membrane.

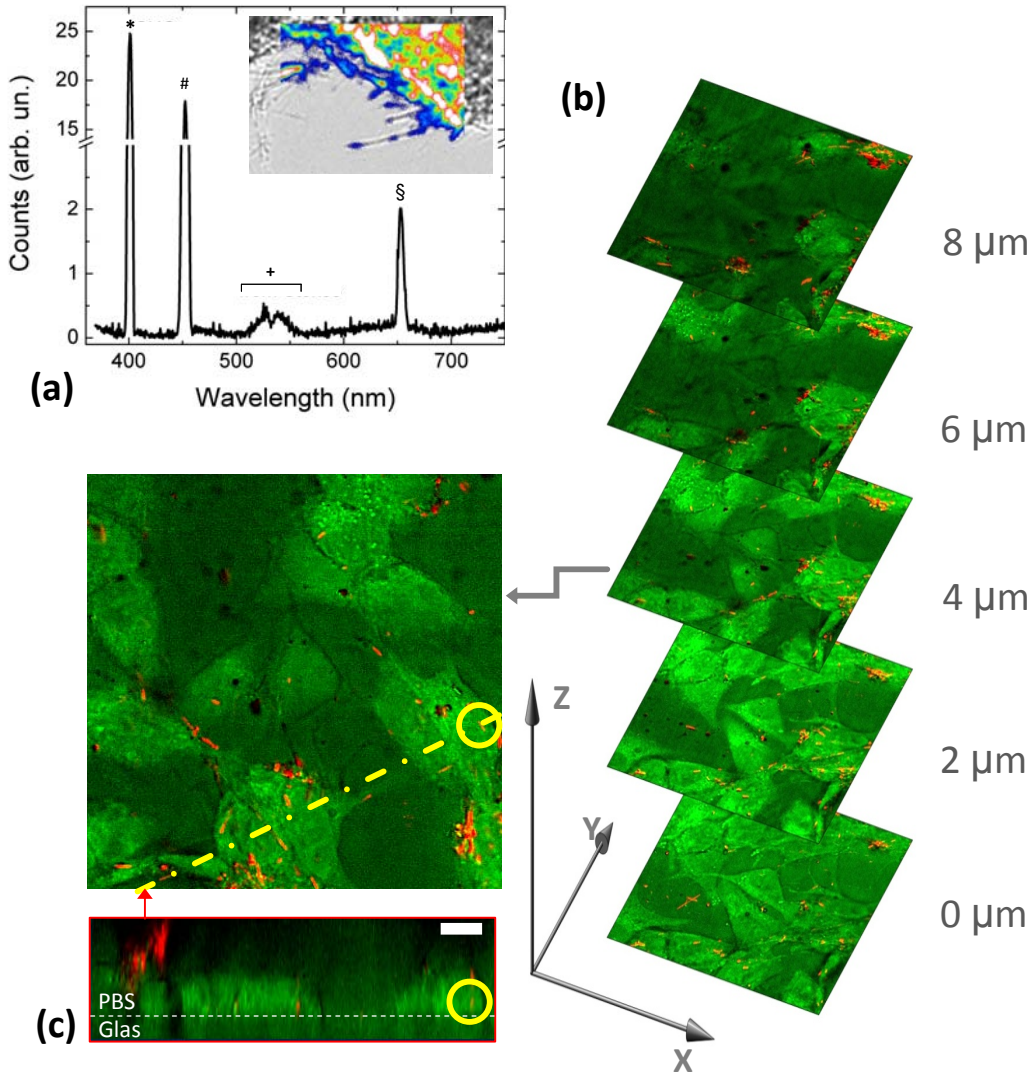

Figure 5. Emission spectrum from a bundle of nanotubes when illuminated with the pump-and-probe and the Stokes beams (a): four distinct bands are discernible originating from: SHG (labeled with *) from the 806-nm beam, SFG (labeled with #) from the combination of the 806 nm beam and the portion of the Stokes beam temporarily overlapping to it (*i.e.*, corresponding to approximately 1045 nm), broadband SHG (labeled with +) from the Stokes beam, and non-resonant CARS signal (labeled with §). SHG when the system was excited at 800 nm was generated outside our detection window. The inset shows a superposition of an image obtained with a transmitted-light microscope of a nanotube bundle and the detected SFG signal. Multimodal *Z*-stacking SH-SY5Y cells treated for 24 h with 20 µg/ml of BNNTs: map of the intensity of the CARS signals from the CH_2 bonds in green, SFG from the nanotubes in red (b); single Z-slice, along a side projection, showing BNNTs inside the cells (single BNNT highlighted by a circle). Scale bar 10 µm.

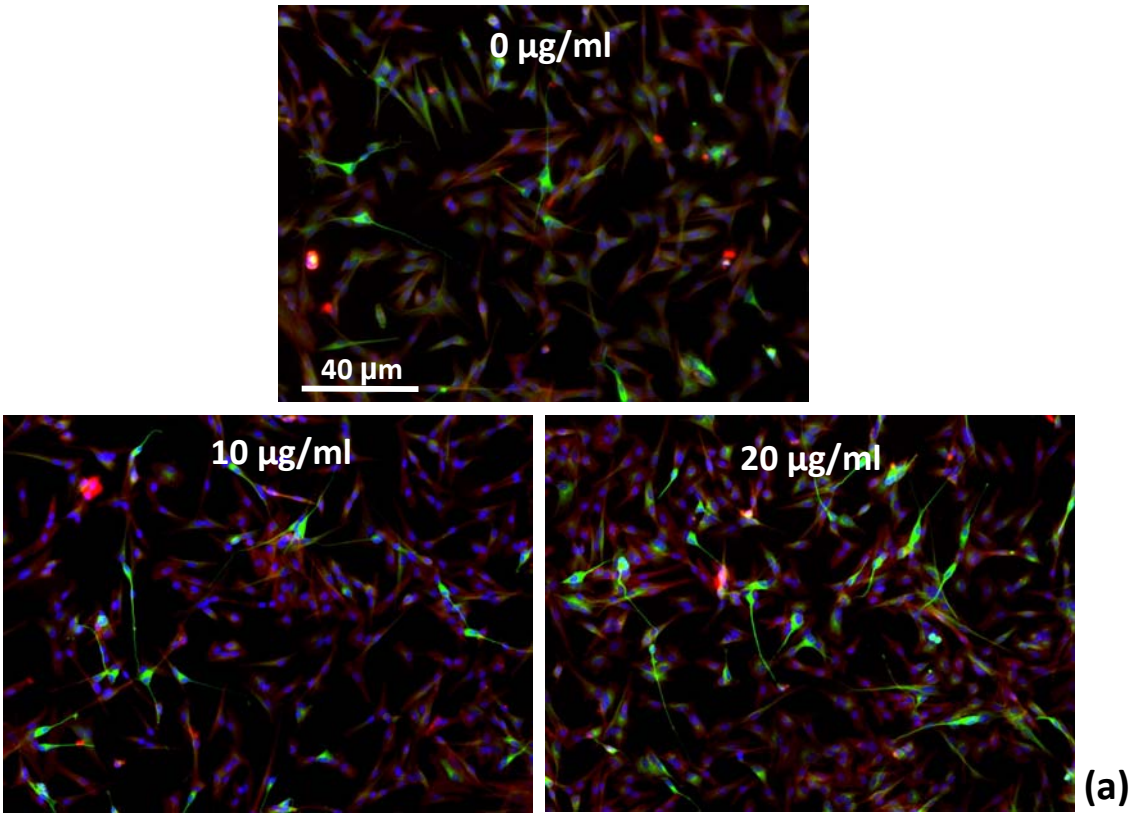

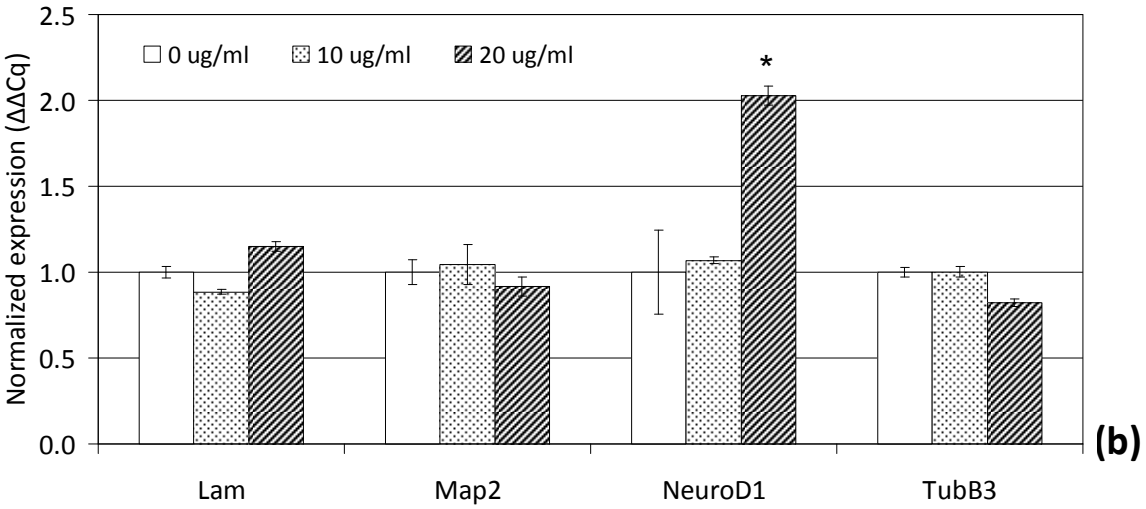

Figure 6. Immunofluorescence analysis of SH-SY5Y cells differentiated for 5 days in the presence of increasing concentrations of BNNTs: β3-tubulin in green, f-actin in red, nuclei in blue (a); qRT-PCR evaluation of transcription of genes involved in SH-SY5Y differentiation following BNNT treatment (b); * $p < 0.05$.

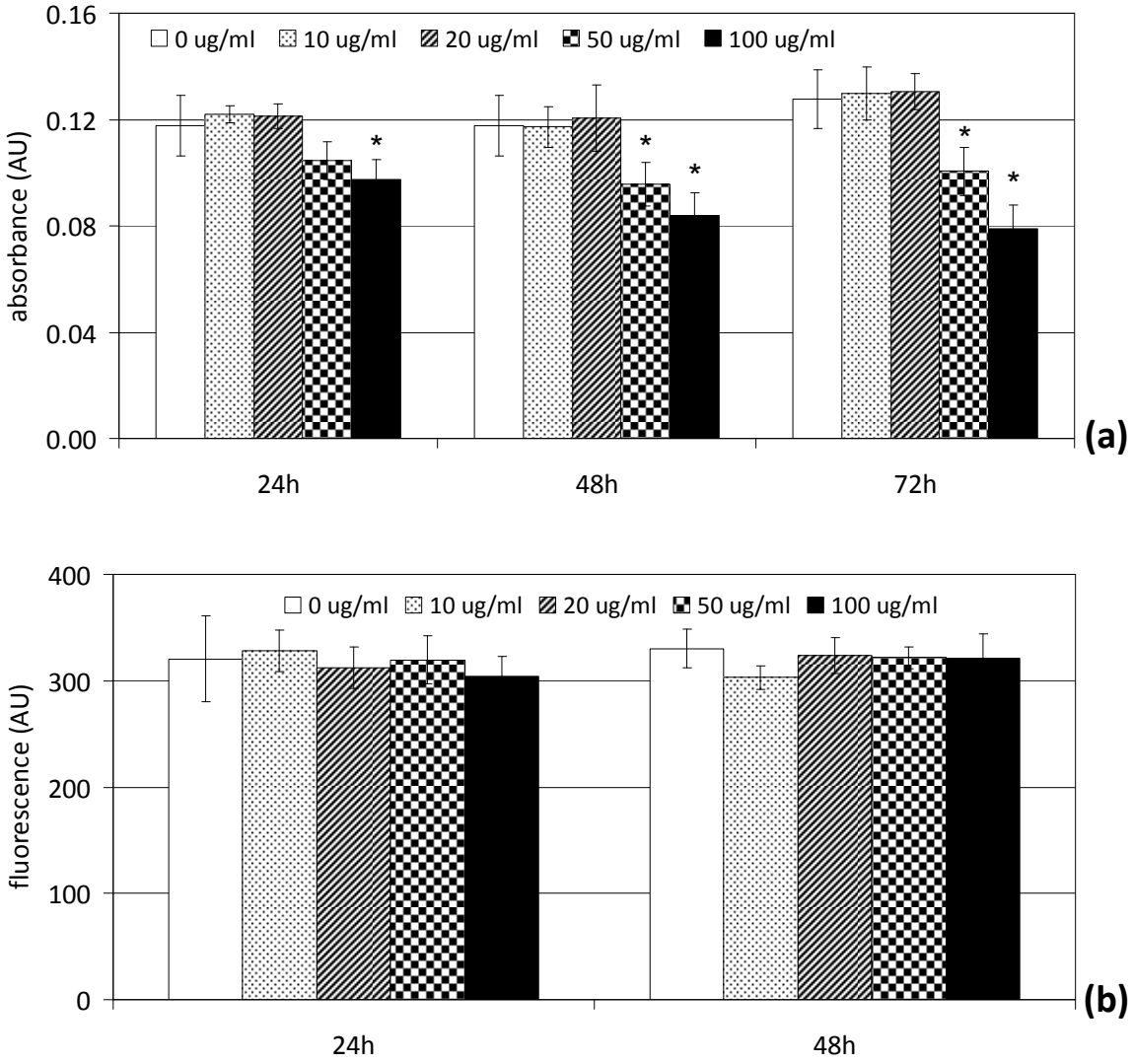

Figure 7. Amido Black assay results of HUVECs treated with 0-100 μg/ml of BNNTs for 24, 48 and 72 h (a); ROS detection on HUVECs treated up to 48 h with the same BNNT concentrations (b). * $p < 0.05$.

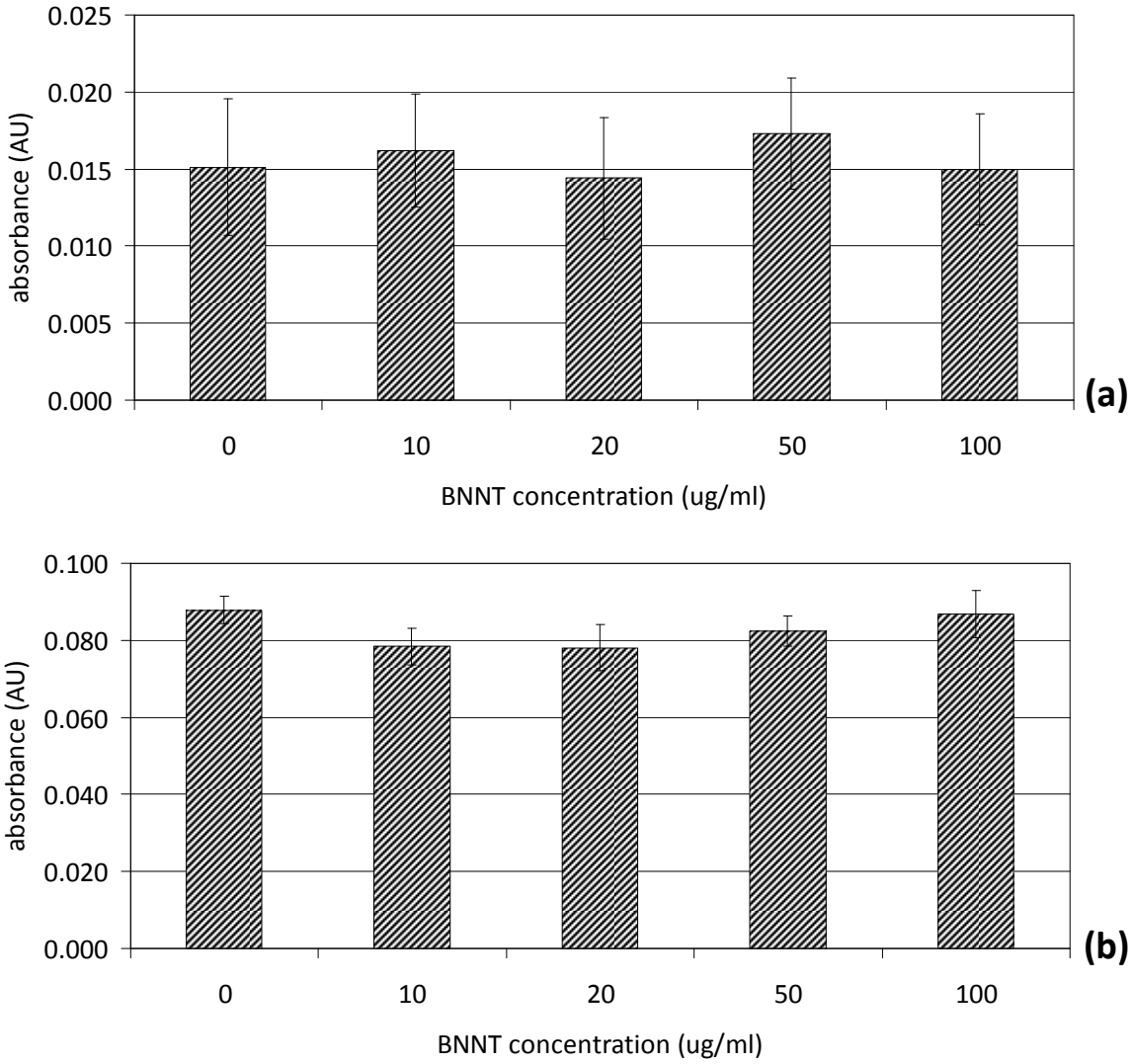

Figure 8. Effects of a 18 h treatment of BNNTs (0-100 μg/ml) on endothelial VCAM-1 (a) and ICAM-1 (b) surface expression.

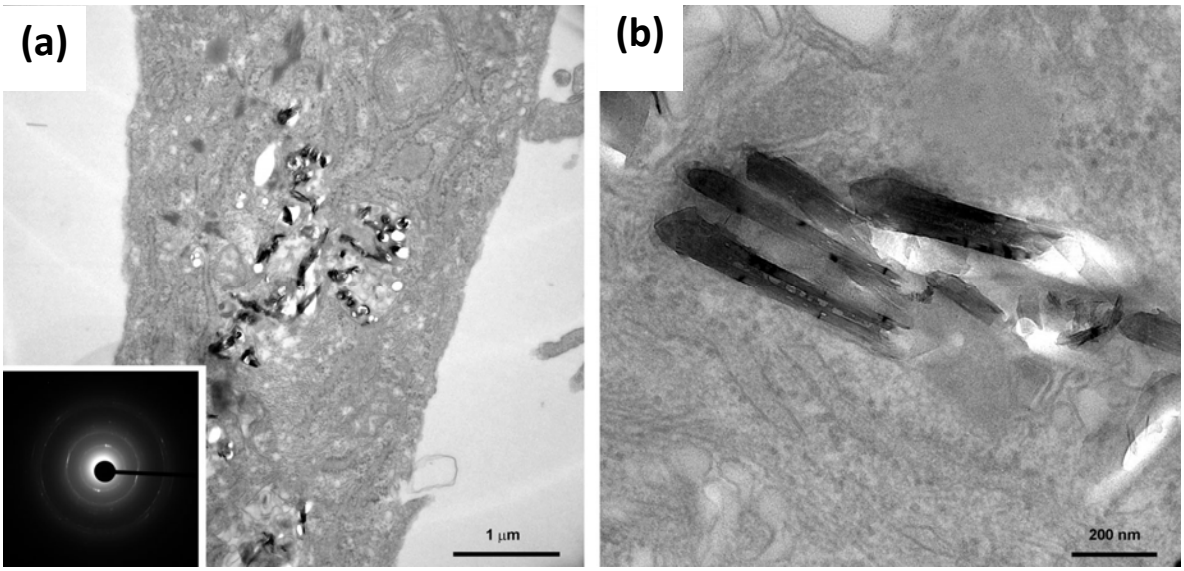

Figure 9. Low (a) and high (b) magnification TEM images of BNNTs internalized by HUVECs. Electron diffraction analysis of BNNTs showed in the inset of (a).

Table 1. Primer sequences for qRT-PCR analysis.

Gene	**Sequence**
Gapdh	5'-CCCTTCATTGACCTCAACTACATG-3' 5'-TGGGATTTCCATTGATGACAAGC-3'
Lam	5'-GCTGCCGAAATGACCTGT-3' 5'-CCCACACTTCCTCTCTCCT-3'
Map2	5'-TCGACTATCAGGTGAACTTTGAA-3' 5'-CCCTGATCTTTCCTGTCCC-3'
NeuroD1	5'-ACCTACTAACAACAAAGGAAATCG-3' 5'-TCCAGCTTGGAGGACCTT-3'
TubB3	5'-GACAATTTCATCTTTGGTCAGAGT-3' 5'-TTCACACTCCTTCCGCAC-3'

Table 2. Quantification of apoptosis in HUVECs exposed to 20 µg/ml of BNNTs for 24, 48, and 72h.

Samples		Viable cells (%)	Necrotic cells (%)	Early apoptotic cells (%)	Late apoptotic cells (%)
24h	Control	91.9±3.5	0.3±0.1	1.9±0.1	5.8±0.8
	BNNTs	92.3±0.6	0.3±0.1	2.4±0.1	4.9±0.4
48h	Control	86.0±0.7	0.7±0.5	6.1±0.2	7.3±0.1
	BNNTs	86.0±0.3	0.8±0.7	6.4±0.2	6.9±0.4
72h	Control	82.5±0.1	0.7±0.6	8.6±0.6	8.2±0.9
	BNNTs	82.6±0.6	1.2±0.6	6.6±0.6	9.4±1.8